applied sciences

MDPI

Article

Mechanism Study on the Intrinsic Damage and Microchemical Interactions of Argillaceous Siltstone Under Different Water Temperatures

Ning Liang [1,2,*], Tao Jin [1,2], Jingjing Zhang [1,2] and Damin Lu [1]

[1] School of Civil Engineering and Architecture, Guangxi University of Science and Technology, Liuzhou 545006, China; 20220301009@stdmail.gxust.edu.cn (T.J.); 20240301014@stdmail.gxust.edu.cn (J.Z.); 100002485@gxust.edu.cn (D.L.)
[2] Guangxi Zhuang Autonomous Region Engineering Research Center of Geotechnical Disaster and Ecological Control, Liuzhou 545006, China
* Correspondence: liangn5@126.com

Abstract: Argillaceous siltstone is prone to deformation and softening when exposed to water, which poses a great threat to practical engineering. There are significant differences in the degrees of damage to this type of rock caused by solutions with different water temperatures. This study aimed to better understand the effect of temperature on argillaceous siltstone by designing immersion tests at water temperatures of 5, 15, 25, and 35 °C, analyzing the mechanical properties and cation concentration shifts under each condition. A water temperature–force coupled geometric damage model for argillaceous siltstone was developed, incorporating a Weibull distribution function and composite damage factors to derive a statistical damage constitutive model. The findings reveal that, with increasing water temperature, the peak strength and elastic modulus of argillaceous siltstone display a concave trend, initially decreasing and then increasing, while the cation concentration follows a convex trend, first increasing and then decreasing. Between 15 and 25 °C, the stress–strain behavior transitions from a four-phase to a five-phase pattern, with pronounced plasticity. The model's theoretical curves align closely with experimental data, with the Weibull parameters m and λ effectively capturing the rock's strength and plastic characteristics. Changes in water temperature notably influence the damage variable D_{12} in the context of water temperature–peak stress coupling, with D_{12} initially increasing and then decreasing with higher temperatures. These research results can provide new methods for exploring the paths of soft rock disasters and provide guidance for designing defenses in geotechnical engineering.

Keywords: argillaceous siltstone; different water temperatures; constitutive model; damage variable

Citation: Liang, N.; Jin, T.; Zhang, J.; Lu, D. Mechanism Study on the Intrinsic Damage and Microchemical Interactions of Argillaceous Siltstone Under Different Water Temperatures. *Appl. Sci.* **2024**, *14*, 11747. https://doi.org/10.3390/app142411747

Received: 4 November 2024
Revised: 10 December 2024
Accepted: 16 December 2024
Published: 16 December 2024

1. Introduction

In the field of geological and geotechnical engineering, the stability of soft rock has consistently been a focus of research due to its complex mineral composition, including kaolinite and montmorillonite; the minerals undergo dissolution, hydrolysis, ion exchange, and redox reactions upon water exposure, altering the rock's microstructure [1]. Shallow groundwater, a vital component of subsurface spaces, experiences temperature variations from external environmental changes, typically ranging from 0 °C to 40 °C [2]. Water temperature changes not only impact the rock's thermodynamic state but also potentially modify the internal moisture distribution, mineral composition, and chemical reaction rates, subsequently affecting both the microstructure and macroscopic mechanical properties of the rock. With global climate change contributing to more frequent extreme weather events, temperature fluctuations in shallow groundwater increasingly threaten the operational safety of underground constructions like tunnels, subways, and underground storage. Especially in clay mineral-rich soft rock formations, these temperature variations

may intensify hydrolysis and ion exchange reactions, weakening rock strength and altering deformation characteristics, potentially leading to mining collapses and landslides (Figure 1). Understanding the impact of water temperature on the mechanical properties of argillaceous siltstone is crucial for predicting and controlling the stability of argillaceous siltstone in practical engineering applications. In industrial fields such as oil and gas extraction and geothermal energy development, knowing the effects of water temperature on rock properties can optimize extraction techniques, reduce resource waste, and improve energy efficiency. This study aims to systematically analyze the effects of shallow groundwater temperature changes on the mechanical properties and microchemical interactions of argillaceous siltstone through experimental testing and theoretical analysis. It is essential not only for revealing the mechanical behavior of argillaceous siltstone under complex environmental conditions but also for ensuring the long-term stability and safety of underground engineering. This research can provide new data and theoretical support for geology, materials science, and environmental science, allowing for a deeper understanding of the reaction mechanisms and evolution processes of argillaceous siltstone under different temperature conditions.

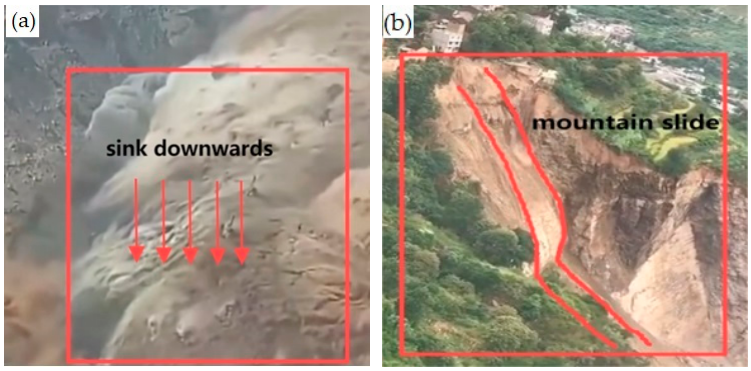

Figure 1. Engineering disaster map. (**a**) Mine collapse. (**b**) Mountain landslide.

There have been extensive scientific investigations into the effects of temperature on rock mechanics. Hongbo Gao et al. conducted mechanical tests on gypsum rock in a high-temperature saline solution, revealing that the rock strength decreases and damage intensifies with an increase in temperature [3]. Zenghui Xu et al. discovered that the peak strength and elastic modulus of fully saturated argillaceous siltstone increase with water temperature [4]. Xiangxin Liu et al., using uniaxial compression tests and scanning electron microscopy (SEM), found that rock strength increases with temperature between 30 °C and 50 °C but slightly declines at higher temperatures, though with minimal variation [5]. Yinlong Lu et al., Using a custom-designed thermostatic water tank within the electro-hydraulic servo-controlled testing system (MTS816), a series of uniaxial compression tests were conducted on sandstone samples immersed at varying temperatures (25 to 95 °C). The study systematically analyzed the water absorption characteristics and the effects of water and temperature on the uniaxial compressive strength (UCS) of the samples. The results revealed that the hydration effect of sandstone is highly sensitive to water temperature. When the water temperature increased from 25 °C to 95 °C, the UCS and elastic modulus of the saturated sandstone increased linearly by 21.3 MPa and 20.2%, respectively [6]. Hui Zhang et al., utilizing damage mechanics theory, constructed a rock damage model under temperature–load coupling, showing that the damage in salt rock escalates with higher temperatures but lessens under higher confining pressure [7]. Chao Wei introduced a thermal damage variable, damage modification coefficients, microfracture compaction coefficients, damage cracking stress, and strain parameters to construct a rock statistical damage constitutive model, based on the Hoek–Brown (H-B) strength criterion with temperature effects [8]. Tianbin Li et al. applied Weibull parameters to create a rock damage statistical constitutive model based on the Drucker–Prager criterion, defining

damage variable [9]. Baoxin Jia et al., utilizing effective stress theory and a segmented function based on the Weibull distribution, developed constitutive models for rock under uniaxial and triaxial compression at high temperatures, achieving close alignment between theoretical outcomes and laboratory curves [10].

Many researchers have delved into the water–rock interaction mechanisms during immersion, primarily focusing on microchemical actions at the water–rock interface. The rock softens as ions in solution interact with the rock's surface, a phenomenon termed ion adsorption [11]. At the microscopic scale, ion adsorption at the water–rock interface primarily manifests in the retention of ions by clay minerals. According to the surface complexation adsorption theory, the surface of soft rock can be considered a polyacid, where hydroxyl groups can release protons and become basic, while cations are viewed as acids, making them prone to surface complexation adsorption at the water–rock interface [12]. Due to the negative charge on the surface of clay minerals, cations are adsorbed at the water–rock interface through Coulombic forces, forming a surface double-layer structure. At the microscopic level, cations enter the hexagonal pores on the siloxane surface and form covalent bonds with the oxygen in Si-O tetrahedra. Through this ion adsorption process, cations from the aqueous solution accumulate at the water–rock interface, awaiting ion exchange with the clay minerals in the rock. Researchers such as Cuiying Zhou et al. observed that cations in soaking solutions initially adsorb onto rock surfaces, causing an initial drop in concentration, and then form water-soluble compounds that dissolve, increasing the cation concentration again, followed by another adsorption phase, with Na^+ changes being particularly notable [13,14]. Yanwei Song et al. analyzed the additional electrical properties and ion adsorption at the soft rock–water interface based on bilayer, ion migration, and nonlinear dynamics theories, but did not quantify interfacial charge and ion adsorption [15–19]. L.P. Qiao et al. investigated the composition, surface charge, and ion exchange of soft rock clay minerals at the water–rock interface using PHREEQ simulations, incorporating mass and charge conservation [20–24]. This study provides valuable insights into the interfacial processes of soft rock.

Despite extensive research into the rock mechanics and water–rock interface chemical interactions during immersion, studies on solution variation primarily consider pH and immersion duration, with limited exploration of water temperature's effects on the chemical behavior and rock mechanics at the water–rock interface. This study addressed this gap by examining the uniaxial mechanical characteristics of argillaceous siltstone under different water temperatures, deriving a damage constitutive model using the Weibull statistical distribution and strain equivalence principles. By validating the model with experimental data, this work highlights changes in water–rock interface chemistry across varying temperatures, contributing to a deeper understanding of soft rock behavior under diverse geological conditions and providing a scientific basis for the safe and effective management of underground engineering projects.

2. Experimental Design

2.1. Preparation of Rock Samples

In this study, argillaceous siltstone was selected as the test material, The weathering degree was classified as medium to slightly weathered, and the core consisted of a mixture of fine-grained sand and clayey silt, X-ray diffraction (XRD) analysis was performed to determine the basic physical parameters and mineral composition of the argillaceous siltstone, as summarized in Table 1. To minimize the variability in the experimental results caused by the heterogeneity of the individual rock samples and to enhance the comparability of the tests, all the rock blocks used in the experiments were extracted from the same geological layer and location within a large, intact rock mass. This careful selection process ensured consistency in the material properties across all the samples.

Table 1. Basic parameters of argillaceous siltstone.

Elastic Moduli E (GPa)	Density ρ (g/cm^3)	Quartz (%)	Albite (%)	Calcite (%)	Potash Feldspar (%)	Anorthite (%)	Clay Minerals (%)
6.51	2.21	42.1	7.5	7.2	15.2	10.4	17.7

The primary minerals of this type of rock are quartz and feldspar, characterized by a brown color and argillaceous-calcite cementation. Using an automatic coring machine, an automatic rock cutting machine, and a double-sided grinding machine, the borehole cores are processed into standard cylindrical specimens (Φ50 mm × 100 mm) through coring, cutting, coarse grinding, and fine grinding. The flatness error of the specimen end faces is no greater than 0.05 mm, and the height, diameter, or side length error of the specimen is no greater than 0.3 mm, as shown in Figure 2.

Figure 2. Argillaceous siltstone samples.

2.2. Experimental Scheme

(1) Soaking Test: To simulate shallow groundwater quality, dilute hydrochloric acid with a pH value of 5.0 was used as the acidic solution. Plastic bottles were utilized as individual containers, each with the same solution volume, and only one rock sample per bottle. The temperature test chamber used was a DW-40 low-temperature test chamber, capable of adjusting temperatures within the range of −55 °C to 80 °C. Based on the geological environment of the area, the test chamber was set to water temperatures of 5 °C, 15 °C, 25 °C, and 35 °C. The plastic bottles containing the rock samples were placed in the low-temperature test chamber and soaked for durations of 1 day, 3 days, 7 days, and 14 days. Before testing, the specimens were dried in an oven at 105 °C for 12 h and subsequently oven-dried at 105 °C for 24 h post-immersion; this was defined as one immersion cycle.

(2) Uniaxial Compression Test: After soaking, uniaxial compression tests were conducted, The instrument used for the uniaxial tests was an electronic universal testing machine (electronic universal testing machine, Shenzhen Sanyuan Zongheng Technology Co., Ltd, Shenzhen, China), with a maximum vertical load capacity of 300 kN. The load measurement error was within ±0.5%, the load resolution was 1/450,000, the displacement measurement error was within ±0.5%, and the displacement resolution was 0.04 μm. The uniaxial compression tests employed a displacement-controlled loading method, with a loading rate set at 0.05 mm/min. Vertical load was applied until the specimen failed, and photographs of the damaged rock were taken.

(3) Microscopic Test: After soaking, the concentrations of Na^+, K^+, and Ca^{2+} ions in the solution were measured using an ion concentration meter, model PXSJ-270F (PXSJ-270F Ion Meter, INESA Scientific Instrument Co., Ltd., Shanghai, China). The ion concentration measurements were accurate to ±0.0001. (The experimental setup is illustrated in Figure 3.)

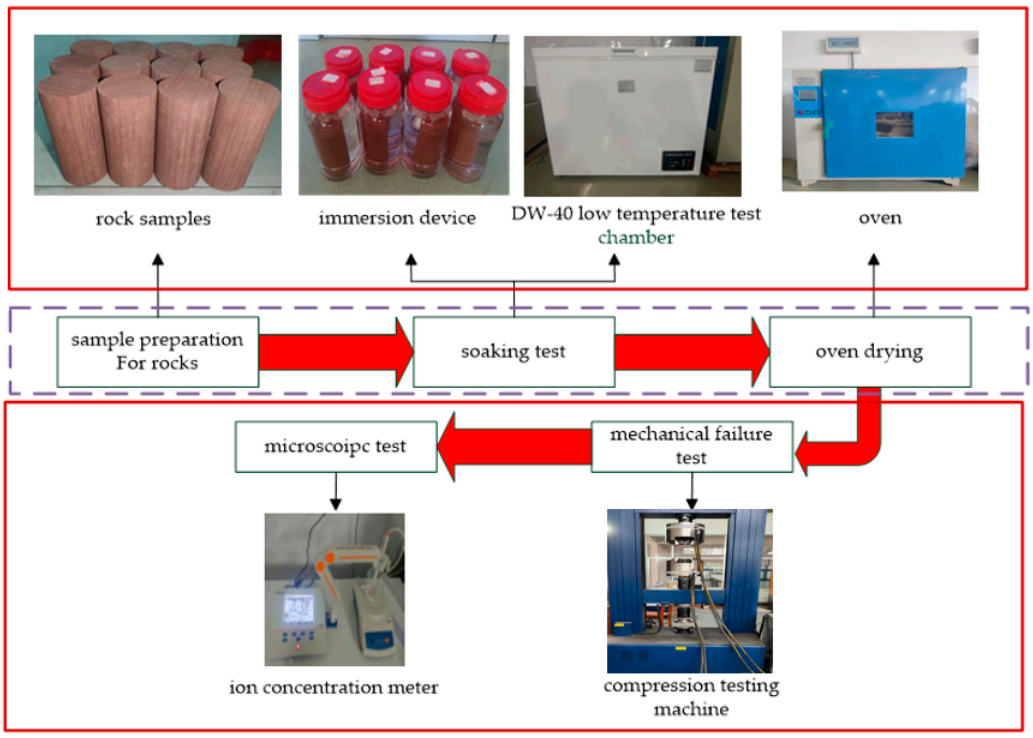

Figure 3. Diagram of the experimental scheme.

3. Experimental Results and Analysis

Mechanical Properties of Argillaceous Siltstone Under Different Water Temperatures

Figure 4 presents the trends in the peak strength and elastic modulus of argillaceous siltstone as a function of water temperature, highlighting distinctive concave curves that clearly illustrate the relationships between temperature and these mechanical properties. As the water temperature increases, both the peak strength and elastic modulus initially decrease, followed by a subsequent increase. Notably, under extreme temperature conditions, specifically at 5 and 35 °C, the peak strength and elastic modulus are significantly higher than at intermediate temperatures of 15 and 25 °C. Additionally, with an extended soaking duration, the temperature's effect on the peak strength and elastic modulus becomes less pronounced. During the initial soaking period (1–3 days), the impact of water temperature on the peak strength and elastic modulus of argillaceous siltstone is very significant. However, as the soaking duration increases, the influence of water temperature on the peak strength and elastic modulus of argillaceous siltstone diminishes.

To investigate the mechanical properties of argillaceous siltstone under varying water temperatures, stress–strain curves were generated after immersion in solutions at different temperatures for 1, 3, 7, and 14 days, as shown in Figure 5. These stress–strain curves not only reveal the deformation characteristics of the rock but also provide foundational data for studying its mechanical properties and establishing its constitutive relationship, particularly characteristics beyond peak compressive strength.

In the early stages of immersion (1–3 days), the stress–strain curve displays four distinct phases: the microcrack compaction phase, elastic deformation phase, plastic yielding phase, and strain-softening phase. During this period, the increase in internal microcracks due to hydration is especially pronounced, highlighting a plastic yielding phase that is absent under natural conditions. Here, the influence of water temperature on the stress–strain curve remains negligible.

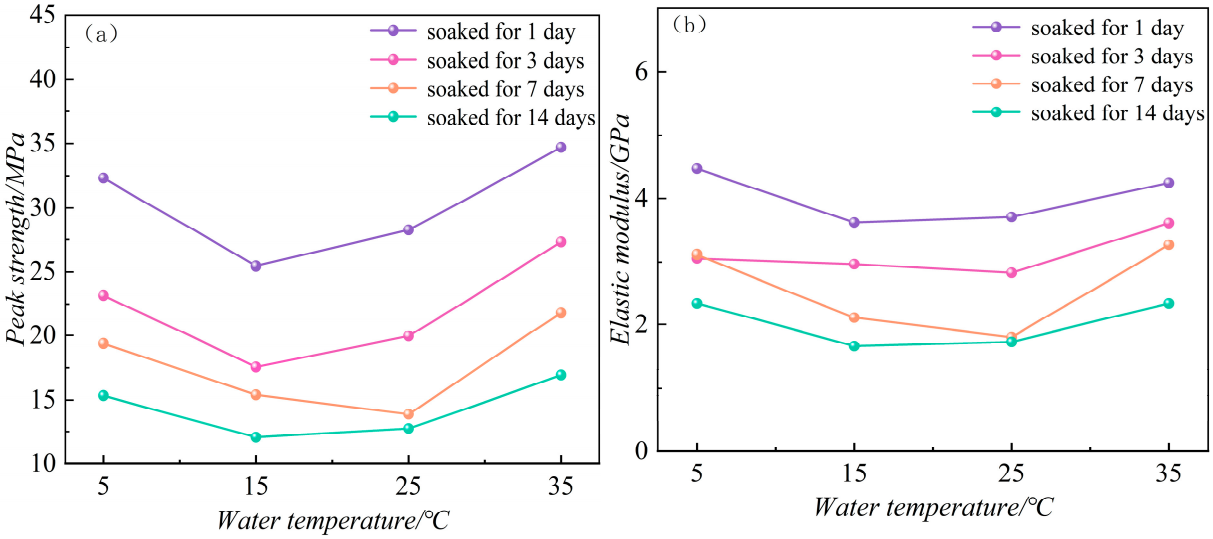

Figure 4. Physical parameters of clay powder under different water temperatures. (**a**) Peak strength. (**b**) Elastic modulus.

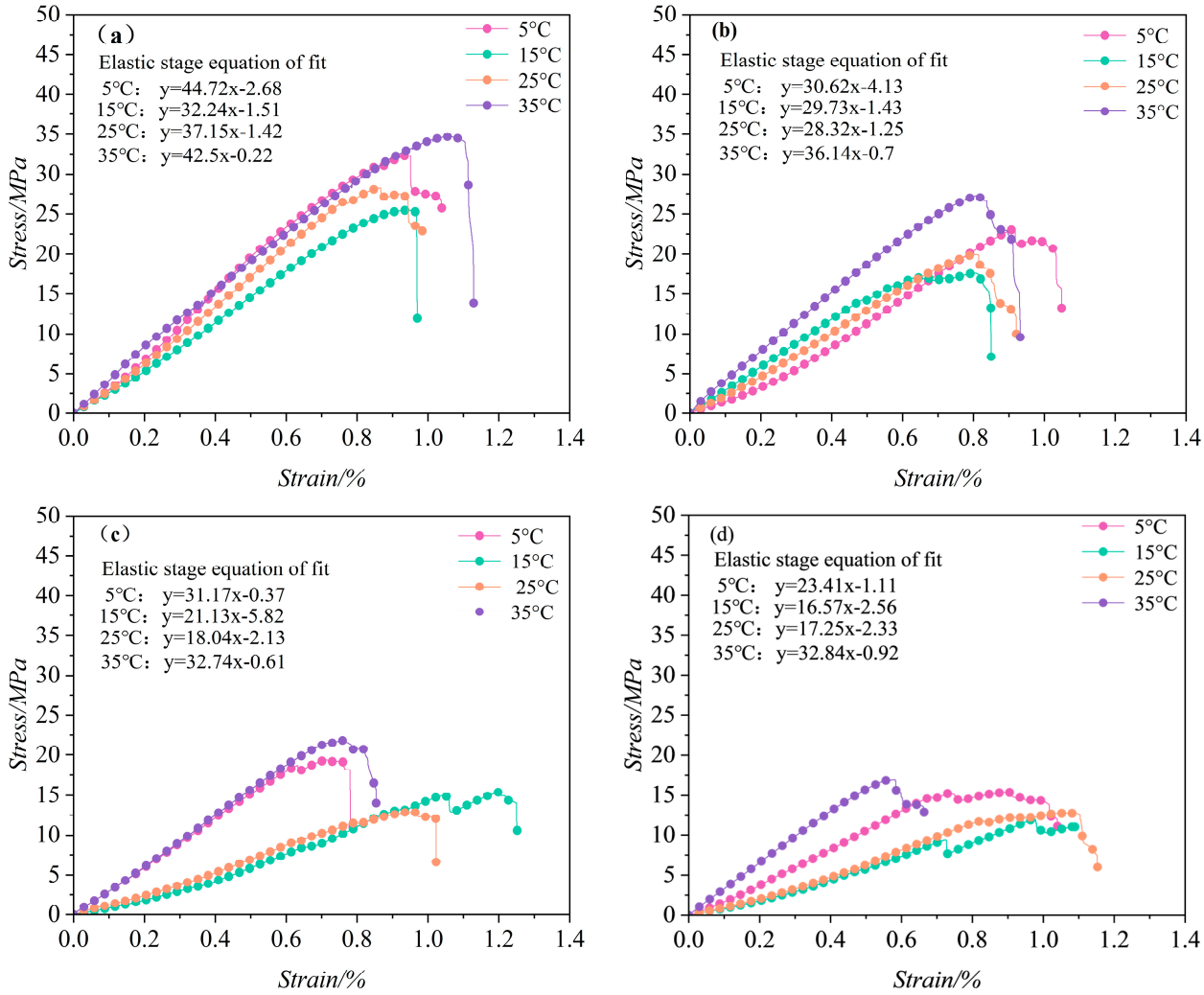

Figure 5. Stress–strain curve of argillaceous siltstone. Soaked for (**a**) 1 day, (**b**) 3 days, (**c**) 7 days, and (**d**) 14 days.

As shown in Figure 5, After 3 days of immersion, specimens soaked at 15 and 25 °C began to exhibit complete five-stage stress–strain curve with increasingly distinct plastic characteristics. This effect intensified with extended immersion time, as hydration and ion exchange between the mineral components and water, along with the adsorption and dissolution of certain minerals, lead to continuous "secondary porosity" formation within the siltstone. Furthermore, in the yielding phase, the increased immersion duration and reduced strength facilitate the micro-rearrangement and slippage of particles under stress, resulting in more rapid propagation of internal cracks compared to the early stages of immersion. This produces a more pronounced extension of the compaction and plastic yielding phases.

The process of microcrack initiation, propagation, and coalescence into macroscopic fractures is the reason for the progressive damage and eventual instability failure of rock specimens. The types of microcracks and macroscopic fractures help reveal the mechanical mechanisms of rock specimen instability and failure under different water temperatures. Based on the failure mechanism, macroscopic fracture types in rocks can be categorized into tensile cracks and shear cracks. Tensile cracks initiate and propagate from the crack tips, extending linearly toward both ends of the rock specimen. If this process continues along an inclined curve, it forms shear cracks. To understand the failure characteristics of argillaceous siltstone in different water temperature solutions, a failure characteristic analysis was conducted on the specimens after failure. As shown in Figure 6, argillaceous siltstone subjected to different water temperatures under uniaxial compression produced more than one obvious failure crack, and the failure surfaces were rough. At water temperatures of 5 °C and 35 °C, the failure mode of argillaceous siltstone was mainly tensile failure, with tensile cracks generated under axial stress that did not penetrate the entire specimen, maintaining a relatively intact state. At water temperatures of 15 °C and 25 °C, the failure mode was primarily "X"-shaped shear failure, with a significant increase in the number of tensile cracks accompanied by the appearance of shear cracks. The tensile cracks initiated and propagated from the crack tips, extending linearly towards both ends of the rock specimen. Eventually, the cracks interconnected, causing severe local damage or even spalling of the rock mass, resulting in a relatively fragmented state of the specimen.

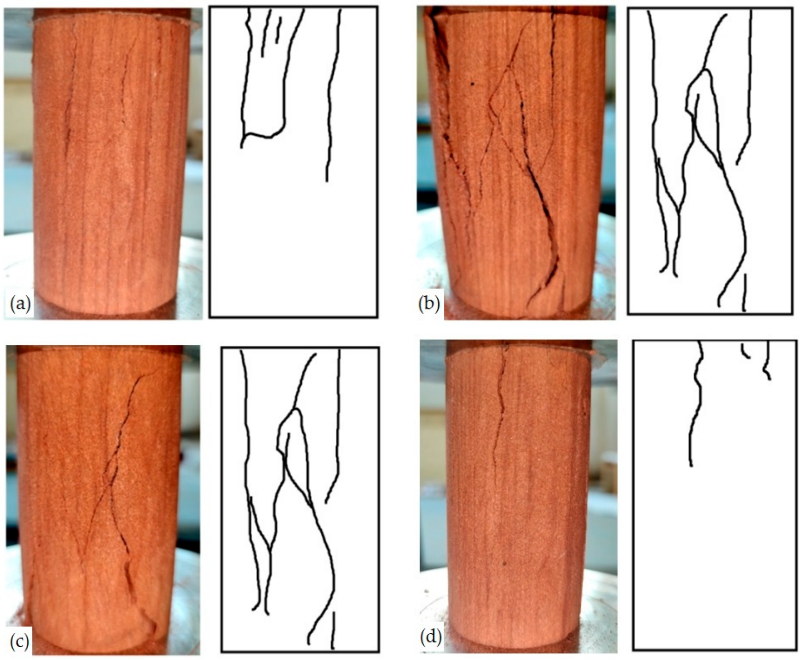

Figure 6. Failure modes of argillaceous siltstone under different water temperatures: (**a**) 5 °C. (**b**) 15 °C. (**c**) 25 °C. (**d**) 35 °C.

In the analysis of rock microstructures, scanning electron microscopy (SEM) plays a crucial role. SEM can reveal the fine structural characteristics of rocks, thereby aiding in the understanding of their mechanical mechanisms. To investigate the microstructural characteristics of argillaceous siltstone under different water temperatures, a field emission scanning electron microscope was used for an in-depth study. The SEM can perform imaging analysis on samples at a magnification of 4000 times. As shown in Figure 7a, after soaking for 3 days, changes in water temperature significantly affect the strength of argillaceous siltstone. Therefore, argillaceous siltstone samples soaked for 3 days under different water temperature conditions were selected for SEM imaging, and the results are shown in Figure 7.

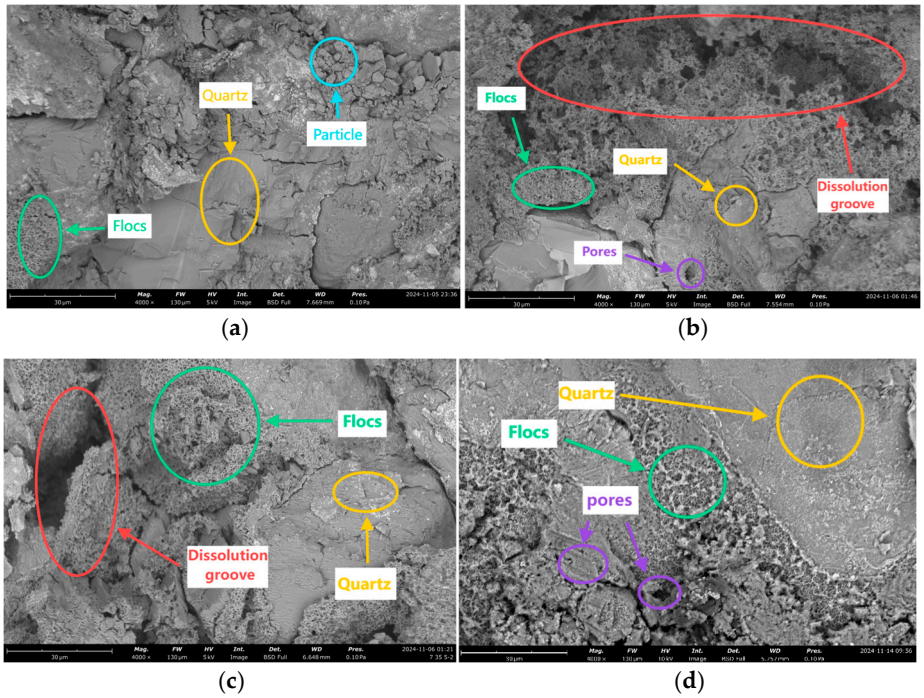

Figure 7. Microstructural images of argillaceous siltstone under the influence of different water temperatures. (**a**) Water temperature at 5 °C. (**b**) Water temperature at 15 °C. (**c**) Water temperature at 25 °C. (**d**) Water temperature at 35 °C.

Figure 5a–d show the microstructures of argillaceous siltstone under water temperatures of 5 °C, 15 °C, 25 °C, and 35 °C, respectively. At 5 °C, parts of the quartz structure have been damaged, and a small amount of flocculent bodies and fine particles appear. These flocculent bodies typically manifest as micron- to millimeter-sized aggregates. As the temperature increases to 15 °C, the degree of damage to the quartz structure further intensifies, forming a large number of flocculent bodies, most of which have been damaged and form corrosion grooves. At 25 °C, the quartz structure shows signs of fracturing, the number of flocculent bodies decreases, and the corrosion grooves become shallower and narrower. At 35 °C, the quartz structure is relatively intact, the flocculent bodies significantly decrease, and their structure shows no evident signs of damage. Due to the significant changes in the internal structure of argillaceous siltstone under different water temperatures, the impact of water temperature on the strength and elastic modulus of argillaceous siltstone becomes very pronounced.

4. Development of a Damage Constitutive Model for Argillaceous Siltstone

4.1. Analysis of the Damage Process

The damage observed in argillaceous siltstone under varying water temperatures mainly arises from chemical interactions between H^+ ions in the solution and the rock's

mineral components. The precipitation of new products from these reactions disrupts the rock's internal structure, leading to a noticeable reduction in load-bearing capacity and a decline in elastic modulus on a macroscopic scale.

In the field of damage mechanics, it is commonly assumed that the material is isotropic. According to Lemaitre's strain equivalence hypothesis, the material's damage can be defined by its effective load-bearing area. Therefore, a micro-element analysis of the argillaceous siltstone at different stages was performed. Let us assume that the micro-element area and nominal stress in the undamaged state are A and σ_1, respectively. After cyclic temperature exposure, the effective area and stress become A_1 and $\sigma_1{}^*$, while following additional damage from loading under the influence of water temperature, they are denoted as A_2 and σ_1 (see Figure 8).

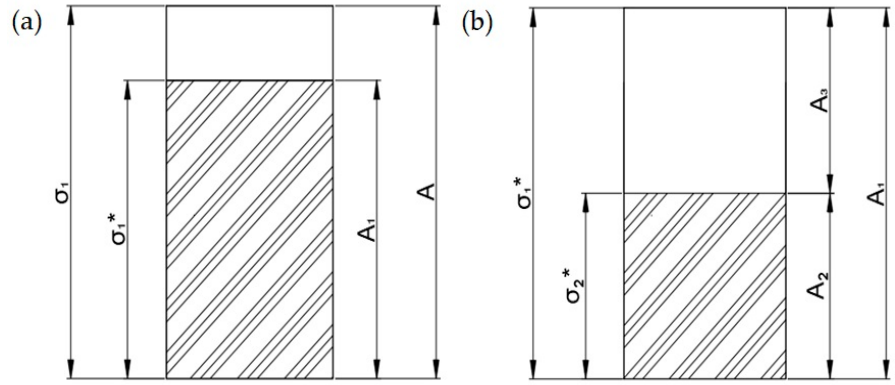

Figure 8. Geometric damage model. (**a**) Damage under different water temperatures without reaching the yield point. (**b**) Load-induced damage beyond the yield point.

Figure 8a depicts the microelement stress state of argillaceous siltstone subjected to water temperature before reaching yield stress. The blank area ($A-A_1$) represents the chemical interaction between H^+ ions in the solution and the mineral components of the rock, indicating the damage caused by water temperature to the argillaceous siltstone. At this point, the blank area signifies the elastic modulus damage D_1 and no longer bears the load. Figure 8b shows the stress state of the microelement after reaching yield stress under the influence of water temperature. It is assumed that the load is applied to the effective area A_1. After reaching the yield point, new cracks initiate within the argillaceous siltstone, gradually extending and eventually forming a fracture surface. At this stage, the area of the blank region (A_1-A_2) indicates the subsequent load-induced damage D_{12}.

By conducting a force analysis on the infinitesimal element in Figure 6a, we can obtain:

$$\sigma_1 A = \sigma_1^* A_1 \tag{1}$$

The damage variable D_1 for argillaceous siltstone under the effect of water temperature can be obtained as:

$$D_1 = 1 - \frac{A_1}{A} \tag{2}$$

The constitutive relationship for damage at this point is:

$$\sigma_1 = \sigma_1^*(1 - D_1) \tag{3}$$

By conducting a force analysis on the infinitesimal element in Figure 5b, we can obtain:

$$\sigma_1^* A_1 = \sigma_2^* A_2 \tag{4}$$

The subsequent damage caused by the load after experiencing water temperature action is denoted as D_2, and $A_3 = A_1 - A_2$; then, we obtain:

$$D_2 = 1 - \frac{A_2}{A_1} \tag{5}$$

$$\sigma_1^* = \sigma_2^*(1 - D_2) \tag{6}$$

The total damage ontological model of argillaceous siltstone at this time can be obtained by combining Equations (3) and (6) as:

$$\sigma_1 = \sigma_2^*(1 - D_{12}) \tag{7}$$

$$\sigma_1 = \sigma_2^*(1 - D_1)(1 - D_2) \tag{8}$$

The total damage variable D_{12} for argillaceous siltstone under water temperature loading is as follows:

$$D_{12} = \frac{A_2}{A} = D_1 + D_2 - D_1 D_2 \tag{9}$$

$$\frac{A_2}{A} = 1 - (1 - D_1)(1 - D_2) \tag{10}$$

According to the generalized Hooke's law,

$$\sigma_2^* = E_0\varepsilon_1 + \mu(\sigma_2 + \sigma_3) \tag{11}$$

Upon substituting Equation (11) into Equation (6) and taking $\sigma_2 = \sigma_3$, we obtain:

$$\sigma_1 = (E_0\varepsilon_1 + 2\mu\sigma_3)(1 - D_{12}) \tag{12}$$

Equation (11) is the total damage ontological model for argillaceous siltstone under water temperature loading.

4.2. Determination of Damage Variable

The effect of water temperature compromises the internal structure of argillaceous siltstone, which is macroscopically reflected as decreases in peak stress, elastic modulus, and related parameters. The elastic modulus, as a representation of the rock's deformation capacity, more effectively captures the extent of damage in argillaceous siltstone. Consequently, the damage variable D_1 induced by water temperature can be defined using the elastic modulus as follows:

$$D_1 = 1 - \frac{E_i}{E_0}, (i = 1, 2, 3 \dots) \tag{13}$$

In this formulation, E_i represents the elastic modulus of argillaceous siltstone after exposure to different water temperatures, while E_0 indicates the elastic modulus in its original state.

From the perspectives of statistical damage mechanics and continuum mechanics, rock damage is viewed as a continuous process, with the microelemental damage of rocks following a statistical distribution. Current research frequently models this microelemental damage using a Weibull distribution. Cao et al. suggest that, under external loads, damage only initiates when these loads reach a specific threshold, a stress–strain state known as the damage threshold [25]. This threshold is further proposed to generally correspond to the yield point. Assuming that the damage to argillaceous siltstone under external loading is a function of axial strain ε_1, with a load damage threshold ε_{1d}, a three-parameter Weibull

distribution is utilized to define the density function for damage beyond the threshold under external load [26]:

$$\phi(\varepsilon) = \frac{m}{\lambda}(\frac{\varepsilon_1 - \varepsilon_{1\mathrm{d}}}{\lambda})^{m-1}\exp[-(\frac{\varepsilon_1 - \varepsilon_{1\mathrm{d}}}{\lambda})^m] \ \ (\varepsilon_1 \geq \varepsilon_{1\mathrm{d}}) \tag{14}$$

In this expression, m and λ denote the shape and scale parameters of the Weibull distribution for the microelements of argillaceous siltstone, respectively. Here, m characterizes the heterogeneity of the material, while λ reflects the rock's plasticity characteristics to some extent. The axial strain ε_{1d} corresponds to the yield point. By integrating this density function, the load-induced damage variable can be obtained.

The expression for D_2 as a function of axial strain ε_1 is as follows:

$$D_2 = \begin{cases} 0 & \varepsilon_1 < \varepsilon_{1\mathrm{d}} \\ 1 - \exp\left[-\left(\frac{\varepsilon_1 - \varepsilon_{1\mathrm{d}}}{\lambda}\right)^m\right] & \varepsilon_1 > \varepsilon_{1\mathrm{d}} \end{cases} \tag{15}$$

The damage of argillaceous siltstone under the combined effects of water temperature and external load is not simply an additive process; rather, it results from a coupling effect. By substituting Equations (13) and (15) into Equation (10), the expression for the total damage variable D_2 of argillaceous siltstone is obtained.

$$D_{12} = \begin{cases} 1 - \frac{E_i}{E_0}\varepsilon_1 < \varepsilon_{1\mathrm{d}} \\ 1 - \frac{E_i}{E_0}\exp\left[-\left(\frac{\varepsilon_1 - \varepsilon_{1\mathrm{d}}}{\lambda}\right)^m\right] \varepsilon_1 > \varepsilon_{1\mathrm{d}} \end{cases} \tag{16}$$

4.3. Constitutive Correction

For Equation (12), when the stress state of the clayey siltstone microelement is at a relatively low stress level, the relationship between σ_1 and ε_1 is linear. This linearity does not align with the initial compressibility phase observed in the stress–strain curve of clayey siltstone obtained from experiments. Therefore, it is necessary to revise the derived constitutive model. Li Xiulei et al. proposed that the total axial void strain of the rock is equal to the intercept of the fitted curve in the elastic deformation phase on the horizontal axis (strain axis) [27]. Additionally, an exponential relationship exists:

$$\varepsilon_{\mathrm{lg}} = \frac{c}{b}(1 - e^{-a\varepsilon_1}) \tag{17}$$

In the expression, ε_{1g} represents the total axial void strain, defined as c/b; ε_1 denotes the axial strain; and c and b are fitting parameters in the elastic deformation phase of the rock's fitting formula. The coefficient a can be determined by fitting the experimental data to this equation ($\varepsilon_1 - (\sigma_1 - 2\mu\sigma_3)/E_i = \varepsilon_{\mathrm{lg}}(1 - e^{-a\varepsilon_1})$). Consequently, the revision of Equation (12) can be expressed as follows:

$$\sigma_1 = \left(E_0\left(\varepsilon_1 - \varepsilon_{\mathrm{lg}}(1 - \exp(-a\varepsilon_1))\right) + 2\mu\sigma_3\right)(1 - D_1)(1 - D_2) \tag{18}$$

By substituting Equations (16) and (17) into Equation (18), we obtain the expression for the triaxial compressive damage constitutive model of the argillaceous siltstone. This model captures the intricate interactions between stress, strain, and damage evolution in the material under various loading conditions, allowing for a comprehensive understanding of its mechanical behavior during triaxial compression tests.

When $\varepsilon_1 < \varepsilon_{1\mathrm{d}}$,

$$\sigma_1 = (E_0(\varepsilon_1 - \varepsilon_{1\mathrm{g}}(1 - \exp(-a\varepsilon_1))) + 2\mu\sigma_3) * \frac{E_i}{E_0} \tag{19}$$

When $\varepsilon_1 \geq \varepsilon_{1d}$,

$$\sigma_1 = \left(E_0\left(\varepsilon_1 - \varepsilon_{lg}\right) + 2\mu\sigma_3\right) \times \frac{E_i}{E_0} \times \exp[-(\frac{\varepsilon_1 - \varepsilon_{ld}}{\lambda})^m] \quad (20)$$

This experiment is a uniaxial compression test; therefore, $\sigma_3 = 0$.

4.4. Determination of Distribution Parameters

There are generally two methods for determining distribution parameters: the linear fitting method and the peak value method [28,29]. The peak value method derives parameter expressions by solving geometric control equations, offering clear physical significance. Therefore, the peak value method was selected for parameter determination. At the peak stress point on the stress–strain curve, two geometric control equations are satisfied:

$$\begin{cases} \sigma_1|_{\varepsilon_1=\varepsilon_p} = \sigma_p \\ \frac{\partial\sigma_1}{\partial\varepsilon_1}|_{\varepsilon_1=\varepsilon_p} = 0 \end{cases} \quad (21)$$

By substituting Equation (4), the expressions for the distribution parameters can be derived, with the parameter values determined according to the methods specified previously.

$$m = \frac{E_i(\varepsilon_p - \varepsilon_{ld})}{(E_i(\varepsilon_p - \varepsilon_{lg}) + 2\mu\sigma_3\frac{E_i}{E_0} - \sigma_r) * \ln(\frac{E_i(\varepsilon_p - \varepsilon_{lg}) + 2\mu\sigma_3\frac{E_i}{E_0} - \sigma_r}{\sigma_p - \sigma_r})} \quad (22)$$

$$\lambda = (\varepsilon_p - \varepsilon_{ld}) * [\ln(\frac{E_t(\varepsilon_p - \varepsilon_{lg}) + 2\mu\sigma_3\frac{E_i}{E_0} - \sigma_r}{\sigma_p - \sigma_r})]^{-\frac{1}{m}} \quad (23)$$

Here, σ_r represents the post-failure strength.

5. Model Validation and Variation in Damage Variable

5.1. Model Validation

To validate the damage constitutive model of argillaceous siltstone under cyclic hydrothermal conditions proposed in this study, experimental data were substituted into Equations (22) and (23). The void strain coefficient a was fitted and solved, resulting in all the parameters of the constitutive equation, as shown in Table 2.

Table 2. Constitutive model parameters.

Water Temperature (°C)	ε_{lg} (%)	ε_{ld} (%)	*a*	*m*	λ	Soaking Duration (d)
5	0.0600	0.48	8.26	3.24	0.26	1
15	0.0460	0.67	7.12	2.79	0.27	
25	0.0370	0.76	9.72	2.95	0.25	
35	0.0018	0.76	6.34	3.32	0.23	
5	0.1200	0.80	5.83	2.72	0.29	3
15	0.0035	0.48	7.29	2.34	0.31	
25	0.0400	0.61	5.34	2.52	0.33	
35	0.0027	0.67	6.56	3.03	0.28	
5	0.0110	0.50	5.98	2.36	0.34	7
15	0.2600	0.84	2.03	2.04	0.44	
25	0.1100	0.62	3.16	1.84	0.41	
35	0.0180	0.55	6.57	2.48	0.31	
5	0.0430	0.68	10.53	2.02	0.36	14
15	0.1500	0.72	6.99	1.44	0.52	
25	0.1300	0.81	4.65	1.64	0.48	
35	0.0047	0.34	10.31	2.23	0.40	

By substituting the constitutive model parameters obtained into Equations (19) and (20), the theoretical stress–strain curve for argillaceous siltstone under different water temperature effects can be derived, as shown in Figure 9. It can be observed that the theoretical curves of the constitutive model align closely with the experimental curves, accurately reflecting the deformation characteristics of argillaceous siltstone.

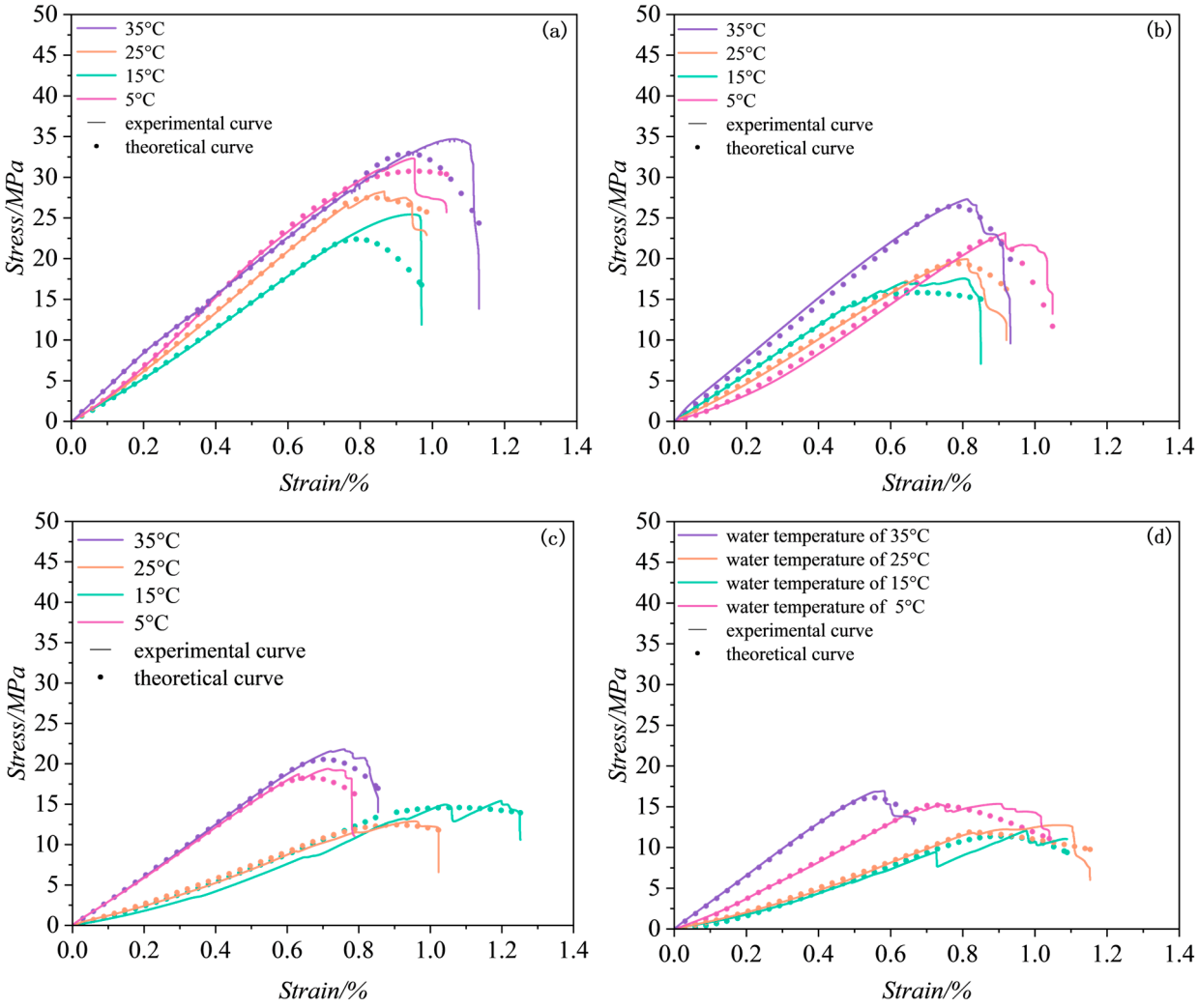

Figure 9. Comparison of experimental and theoretical curves. Soaked for (**a**) 1 day, (**b**) 3 days, (**c**) 7 days, and (**d**) 14 days.

5.2. Evolution Law of Parameters m and λ in Damage Variable Under the Action of Different Water Temperatures

The parameter λ lambda represents the scale parameter in the Weibull distribution function, which determines the scale or range of the distribution. In a physical sense, it can, to some extent, reflect the plastic characteristics of the rock. The shape parameter mm indicates the degree of material homogeneity, where a higher m value suggests greater homogeneity in the mechanical properties of the rock, while a lower m value indicates lesser homogeneity [30]. As shown in Figure 10, When the water temperature is between 5 °C and 15 °C, the shape parameter m decreases with rising water temperature, leading to a decrease in strength. Conversely, between 15 °C and 35 °C, the shape parameter m increases with rising water temperature, resulting in an increase in strength. The trend of the scale parameter λ with increasing water temperature is opposite to that of the shape parameter m. When the water temperature is near room temperature (15–25 °C), the scale parameter λ increases, indicating that the plastic characteristics of argillaceous siltstone

become more pronounced. Between 5 °C and 15 °C, as the water temperature rises, the scale parameter λ increases. However, between 15 °C and 35 °C, as the water temperature rises, the scale parameter λ decreases, indicating a reduction in the plastic characteristics of argillaceous siltstone.

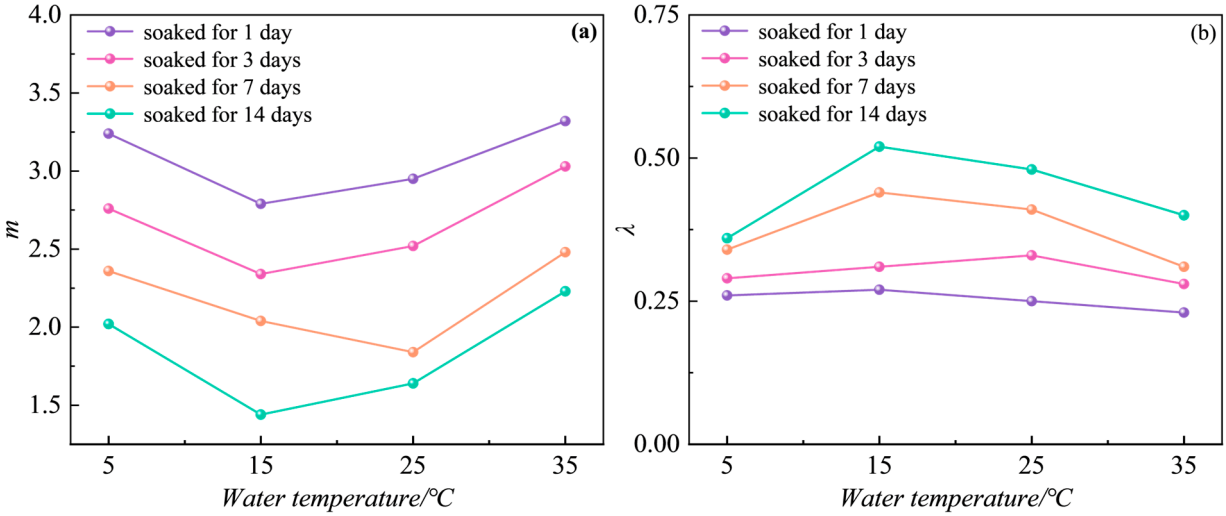

Figure 10. The variation patterns of the constitutive model parameters m and λ. (**a**) The variation pattern of parameter m. (**b**) The variation pattern of parameter λ.

To investigate the variations of damage variables D_{12} under the coupled action of water temperature and peak stress, and D_3 under the action of peak stress (where D_3 is the difference between the total damage variable D_{12} under the action of water temperature and peak load and the elastic modulus damage variable D_1 under the action of water temperature) for argillaceous siltstone soaked at different water temperatures, a graph of the relationships between elastic modulus damage variable D_1, damage variable D_{12}, and damage variable D_3 with water temperature was plotted, as shown in Figure 11. In the early stage of soaking (1–3 days), changes in water temperature have little effect on damage variable D_1, which generally shows an initial increase followed by a decrease with increasing water temperature. This change becomes more pronounced with prolonged soaking. For damage variable D_{12}, the trend is generally consistent with that of D_1; however, the magnitude of change is inversely proportional as soaking time increases. In the early soaking stage (1–3 days), water temperature significantly affects D_{12}, but this effect diminishes with longer soaking times. This phenomenon can be attributed to the significant changes in the internal structure of argillaceous siltstone with prolonged soaking and varying water temperatures. Under loading, the internal pores of the argillaceous siltstone are compressed, leading to increased densification. However, the degree of softening caused by different water temperatures varies, particularly in the early soaking stage (1–3 days), resulting in the observed effects.

The damage variable D_3 indicates the degree of deterioration of argillaceous siltstone after soaking; a smaller D_3 value signifies greater damage. As illustrated in Figure 11, the D_3 value decreases progressively with increased soaking time, indicating that the damage to argillaceous siltstone intensifies as soaking time extends.

During the soaking process at different water temperatures, chemical reactions between the minerals in argillaceous siltstone and water lead to changes in cations (such as Na^+ and Ca^{2+}). These reactions involve the hydrolysis of minerals with water. Additionally, during hydration, the minerals in argillaceous siltstone absorb water, swell, and adsorb various ions. The release and migration of these ions reduce the rock's cohesion and shear strength, leading to a decline in the overall mechanical properties of the soft rock, which makes it more prone to softening and even disintegration. To gain a deeper understanding of the mechanisms of water–rock microchemical interactions influenced

by water temperature, it is essential to investigate the changes in cation concentrations in argillaceous siltstone during soaking at different water temperatures.

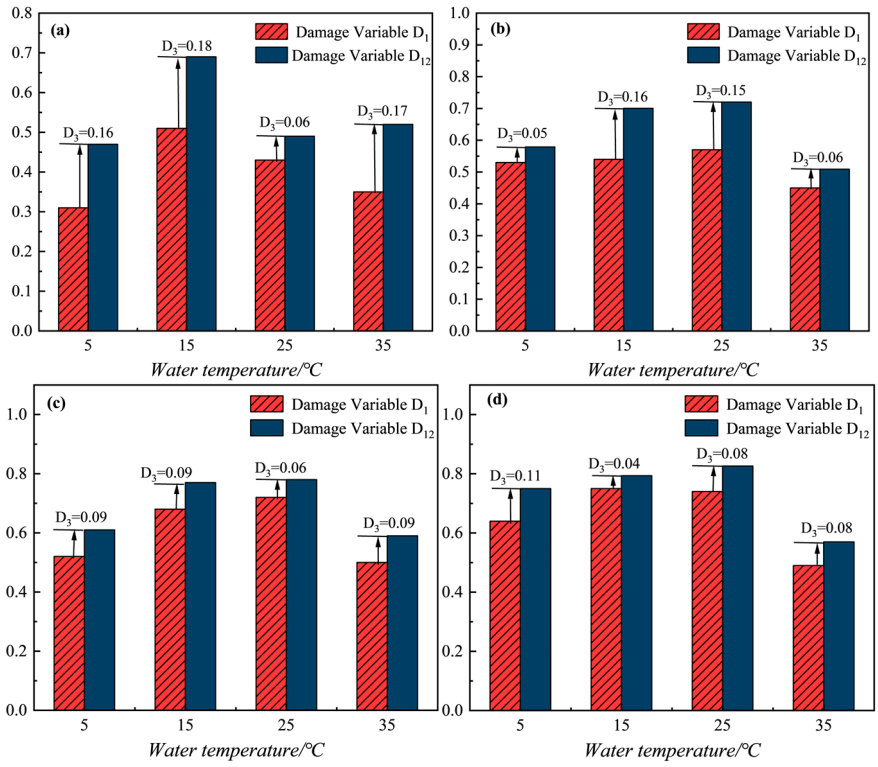

Figure 11. Bar chart representing damage variables D_1 and D_{12}. Soaked for (**a**) 1 day, (**b**) 3 days, (**c**) 7 days, and (**d**) 14 days.

6. Study on the Mechanism of Microscopic Chemical Interactions at Different Water Temperatures

Variation in Cation Concentrations in Solution Under Different Water Temperatures

Existing studies have indicated that water–rock chemical interactions primarily manifest as chemical reactions and ion adsorption, as shown in Figure 12 [9,10].

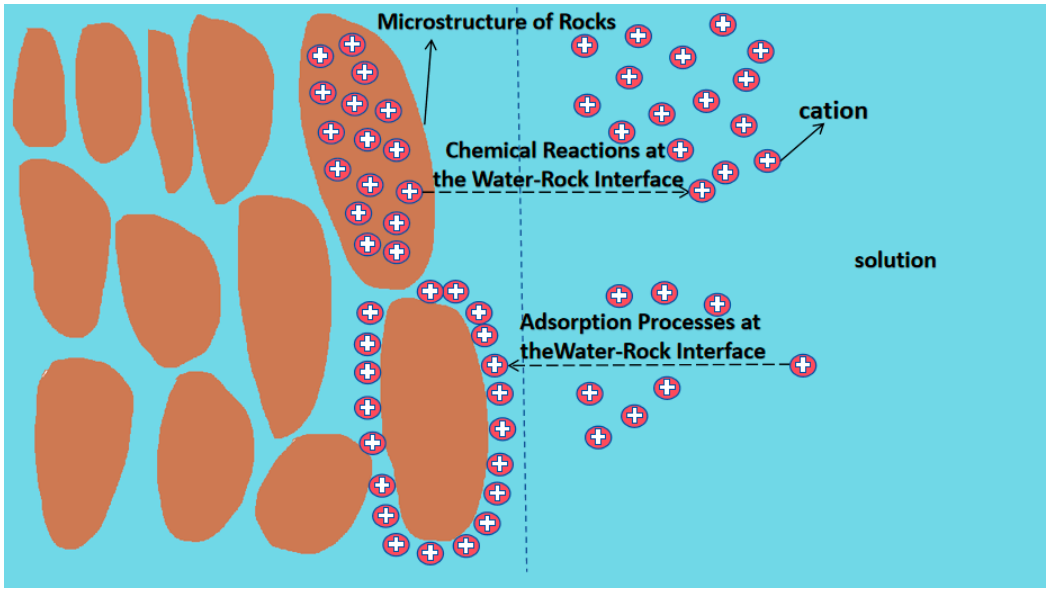

Figure 12. Chemical reactions and adsorption processes at the water–rock interface.

To investigate the variations in cation concentrations during the immersion of argillaceous siltstone in different solutions, the concentration change curves for cations were plotted, as shown in Figure 13.

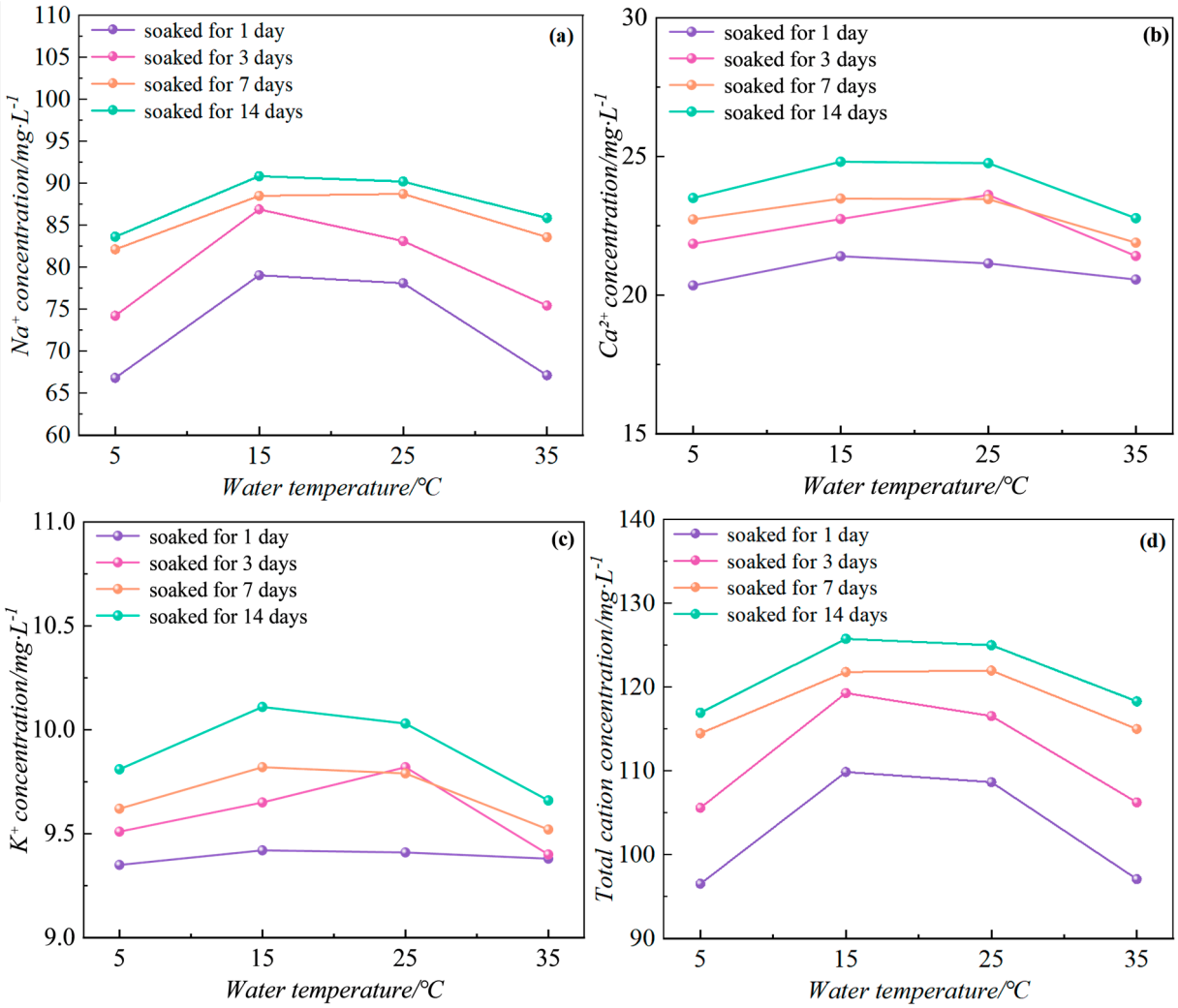

Figure 13. Change curves of cation concentrations in solutions at different temperatures. (**a**) Na^+. (**b**) Ca^+. (**c**) K^+. (**d**) Total cations.

(1) Overall, the concentrations of Na^+, K^+, and Ca^{2+} in the solution exhibit similar trends in relation to water temperature; as the temperature rises, their concentrations initially increase and then decrease. Notably, the concentration curve for Na^+ shows minimal variation as the duration of immersion increases.

(2) During the initial immersion period (1–3 days), there is a significant increase in the total concentration of cations in the solution, indicating a strong chemical interaction between water and rock. After 3 days of immersion, the increase in total cation concentration begins to slow down, suggesting a weakening of the chemical interaction.

(3) As the water temperature increases, the overall trend of total cation concentration first increases and then decreases. In low-temperature solutions (5–15 °C), there is a significant rise in total cation concentration, reaching a peak at 15 °C. In medium to high temperatures (15–35 °C), there is a notable decline. This is primarily due to the combined effects of hydrolysis and adsorption interactions at the water–rock interface. In low-temperature solutions (5–15 °C), adsorption is the dominant process. As the water temperature rises, cations adsorbed on the rock surface gradually detach, leading to an increase in the total cation concentration in the solution. However, in medium to high

temperatures (15–35 °C), exchange processes become dominant. As the water temperature continues to rise, the hydrolysis reactions between water and rock decrease, resulting in a decrease in the total cation concentration in the solution.

7. Conclusions

This study focused on argillaceous siltstone, conducting uniaxial failure tests and microscopic chemical experiments under varying water temperatures. The research investigated the damage to argillaceous siltstone and changes in cation concentration in the solution at different water temperatures. Based on these findings, a damage constitutive model for argillaceous siltstone under varying water temperatures was established, and the evolution of its damage variable was analyzed. The results obtained are as follows:

(1) With increasing water temperature, the peak strength and elastic modulus of argillaceous siltstone exhibit a "concave" trend, initially decreasing and then increasing, while the cation concentration in the solution shows a "convex" trend, first rising and then falling. The flocculent structures within the mesoscopic interior of the argillaceous siltstone initially increase and then decrease. Integrating both microscopic and mesoscopic studies, it is evident that the chemical interactions between water and rock are highly significant under water temperatures ranging from 5 °C to 25 °C, while these interactions gradually weaken at temperatures between 25 °C and 35 °C.

(2) Based on the constructed temperature–stress coupling damage variable, and taking into account factors such as the initial compaction stage and damage threshold, a uniaxial compression damage constitutive model for argillaceous siltstone under different water temperatures was established. The Weibull parameters within this model partially reflect the strength and plasticity characteristics of argillaceous siltstone, and the theoretical results are largely consistent with laboratory findings.

(3) With the increase in water temperature, the variation trends of damage variables D_1 and D_{12} are generally consistent. Overall, damage variable D_1 first increases and then decreases with the rise in water temperature. In the initial soaking period (1–3 days), the impact of water temperature on damage variable D_1 is not significant. However, as the soaking duration increases, this effect becomes more pronounced. Conversely, the variation of damage variable D_{12} is opposite to that of D_1. Damage variable D_3 indicates the degree of degradation of argillaceous siltstone after soaking. As the soaking duration increases, damage variable D_3 gradually decreases, indicating that the extent of degradation in argillaceous siltstone increases with longer soaking times.

These findings have important implications for practical engineering applications, such as tunnel excavation and underground storage construction. By understanding the effect of temperature on the mechanical properties of argillaceous siltstone, engineering design and risk assessment can be better conducted.

This research has achieved excellent results, but there are still the following shortcomings:

In the stress–strain curves, when the argillaceous siltstone undergoes the failure stage, the change in its curve is not very ideal, resulting in poor fitting in the failure stage. In the future, the constitutive model can be improved by adding new parameters to achieve better fitting.

This paper only analyzes the effects of different water temperatures on argillaceous siltstone. In the future, the effects of different water temperatures on clay-rich rocks can be analyzed.

Author Contributions: Conceptualization, N.L. and D.L.; data curation, T.J.; formal analysis, N.L. and D.L.; funding acquisition, N.L.; investigation, T.J. and J.Z.; methodology, T.J. and J.Z.; resources, N.L. and D.L.; validation, T.J.; writing—original draft, N.L. and T.J.; writing—review and editing, N.L., T.J., and J.Z. All authors have read and agreed to the published version of the manuscript.

Funding: This research was funded by the Guangxi Science and Technology Base Talent Project (AD21220126, AD23026255), the Basic Ability Enhancement Program for Young and Middle-Aged

Teachers of Guangxi (2021KY0358, 2023KY0346), and the Guangxi University of Science and Technology Doctoral Fund Project (21z53).

Institutional Review Board Statement: Not applicable.

Informed Consent Statement: Not applicable.

Data Availability Statement: The original contributions presented in the study are included in the article, further inquiries can be directed to the corresponding author.

Conflicts of Interest: The authors declare no conflicts of interest.

References

1. Zhou, H.K.; Zheng, D.; Liu, J.F.; Yin, R.Q. Fractal Characterization of the Microsgture of Red-Bed Soft Rocks and Kinetic Modeling of Interfacial Evolution. *Appl. Sci.* **2024**, *14*, 4458. [CrossRef]
2. Kurylyk, B.L.; Bourque, C.P.A.; MacQuarrie, K.T.B. Potential surface temperature and shallow groundwater temperature. *Hydrol. Earth Syst. Sci. Discuss.* **2013**, *10*, 3283–3326.
3. Gao, H.B.; Liang, W.G.; Yang, X.Q. Experimental study on mechanical properties of gypsum rock under high-temperature salt solution immersion. *J. Rock Mech. Eng.* **2011**, *30*, 935–943.
4. Xu, Z.H.; Liu, G.T.; Ye, Y.X. Experimental study on the effect of temperature on permeability coefficient of soft rock. *J. China Three Gorges Univ.* **2006**, *4*, 301–304.
5. Liu, X.X.; Liang, Z.Z.; Zhang, Y.B. Influence of water temperature on the physical and mechanical properties of argillaceous siltstone. *Chin. J. Undergr. Space Eng.* **2014**, *10*, 586–592.
6. Lu, Y.; Wang, L.; Sun, X. Experimental study of the influence of water and temperature on the mechanical behavior of mudstone and sandstone. *Bull. Eng. Geol. Environ.* **2017**, *76*, 645–660. [CrossRef]
7. Zhang, H.M.; Lei, L.N.; Yang, G.S. Rock damage model under temperature and load. *J. Rock Mech. Eng.* **2014**, *33*, 3391–3396.
8. Wei, C.; Zhao, C.; Zhao, C. Constitutive model of rock statistical damage considering temperature effect and validation. *J. Cent. S. Univ.* **2024**, *55*, 1056–1067.
9. Li, T.; Gao, M.; Chen, G. Brittle evaluation method of hard rock based on thermal-mechanical damage constitutive parameters. *J. Rock Mech. Eng.* **2022**, *41*, 2593–2602.
10. Jia, B.; Chen, G.; Liu, F. Damage constitutive model and validation of rock at high temperatures. *Rock Soil Mech.* **2022**, *43*, 63–73.
11. Maugeri, M.; Ragusa, A.; Torrisi, M. Underground pollution: Some solutions of the transport equation. *Math. Comput. Model.* **2003**, *37*, 583–587. [CrossRef]
12. Zhang, Z.J.; Zhou, Q.; Yuan, Z.T. Adsorption of Mg^{2+} and K^{+} on the kaolinite (001) surface in aqueous systems: A combined DFT and AIMD study with experimental verification. *Appl. Surf. Sci.* **2021**, *538*, 1480–1495. [CrossRef]
13. Zhou, C.Y.; Deng, Y.M.; Tan, X.S. Study on the changes of chemical composition of solution in the process of water saturation of soft rock. *J. Rock Mech. Eng.* **2004**, *22*, 3813–3817.
14. Zhou, C.Y.; Tan, X.S.; Deng, Y.M. Study on the microscopic mechanism of soft rock softening. *J. Rock Mech. Eng.* **2005**, *3*, 394–400.
15. Song, Y.J.; Zheng, Y.; Jiang, L.J. Theoretical model of double layer conductivity of mixed argillaceous sandstone. *Well Logging Technol.* **2008**, *32*, 197–202.
16. Zuddas, P.; Censi, P.; Inguaggiato, C. The behaviour of zirconium and hafnium during water-rock interaction. *Appl. Geochem.* **2018**, *94*, 46–52. [CrossRef]
17. Oh, Y.S.; Jo, H.Y.; Ryu, J.H. A microfluidic approach to water-rock interactions using thin rock sections: Pb and U sorption onto thin shale and granite sections. *J. Hazard. Mater.* **2017**, *324*, 373–381. [CrossRef] [PubMed]
18. Eang, K.E.; Igarashi, T.; Kondo, M. Groundwater monitoring of an open-pit limestone quarry: Water-rock interaction and mixing estimation within the rock layers by geochemical and statistical analyses. *Int. J. Min. Sci. Technol.* **2018**, *28*, 849–857. [CrossRef]
19. Tabbagh, A.; Cosenza, P. Effect of microstructure on the electrical conductivity of clay-rich systems. *Phys. Chem. Earth* **2007**, *32*, 154–160. [CrossRef]
20. Qiao, L.P.; Anda, H.; Wang, Z.C. Alteration of minerals and temporal evolution of solution in reactive flow through granitic rock fractures. *Int. J. Rock Mech. Min. Sci.* **2019**, *123*, 284–296. [CrossRef]
21. Ling, S.X.; Wu, X.Y.; Sun, C.W. Experimental study on chemical damage and mechanical deterioration of black shale under water-rock chemical interaction. *Exp. Mech.* **2016**, *31*, 511–524.
22. Leng, X.L.; Wang, C.; Pang, R. Material preparation and geotechnical properties of transparent cemented soil for physical modeling. *Front. Mater.* **2021**, *8*, 740388. [CrossRef]
23. Aochi, Y.O.; Farmer, W.J. Effects of surface charge and particle morphology on the sorption/desorption behavior of water on clay minerals. *Colloids Surf. A Physicochem. Eng. Asp.* **2011**, *374*, 22–32. [CrossRef]
24. Wu, H.H.; Liu, P.H.; Gao, S. Interfacial reaction characteristics of kaolinite-water solutions. *Sci. Cit. Index* **2005**, *34*, 410–416.
25. Cao, W.G.; Zhao, H.; Li, X. Statistical damage model with strain softening and hardening for rocks under the influence of voids and volume changes. *Can. Geotech. J.* **2010**, *47*, 857–871. [CrossRef]
26. Zhang, C.; Yang, C.; Bai, Y. Study on damage evolution analysis and modeling methods of brittle materials in rock. *Rock Soil Mech.* **2021**, *42*, 2344–2354.

27. Li, X.; Chen, H.; Zhang, J. Constitutive model of the whole deformation process of rock considering initial void compaction. *J. Southwest Jiaotong Univ.* **2022**, *57*, 314–321.
28. Cao, W.; Fang, Z.; Tang, X. Study on statistical constitutive model of rock damage and softening. *J. Rock Mech. Eng.* **1998**, *06*, 628–633.
29. Jiang, H.; Jiang, A.; Yang, X. Statistical damage constitutive model of high-temperature rock based on Weibull distribution and its verification. *Rock Soil Mech.* **2021**, *42*, 1894–1902.
30. Xu, X.L.; Yue, C.Q.; Xu, L.Q. Thermal damage constitutive model and brittleness index based on energy dissipation for deep rock. *Mathematics* **2022**, *10*, 410. [CrossRef]